*J. Fluid Mech.* (1998), *vol.* 363, *pp.* 153–171. Printed in the United Kingdom



# Experiments on the stabilization of the no-motion state of a fluid layer heated from below and cooled from above

By JIE TANG† AND H. H. BAU‡

Department of Mechanical Engineering and Applied Mechanics, University of Pennsylvania, Philadelphia, PA, 19104-6315, USA

(Received 6 January 1997 and in revised form 28 July 1997)

It is demonstrated experimentally that through the use of feedback control, it is possible to stabilize the no-motion (conductive) state of a fluid layer confined in a circular cylinder heated from below and cooled from above (the Rayleigh–Bénard problem), thereby postponing the transition from a no-motion state to cellular convection. The control system utilizes multiple sensors and actuators. The actuators consist of individually controlled heaters microfabricated on a silicon wafer which forms the bottom of the test cell. The sensors are diodes installed at the fluid's midheight. The sensors monitor the deviation of the fluid temperatures from preset, desired values and direct the actuators to act in such a way as to eliminate these deviations.

## 1. Introduction

The ability to control complex convective flow patterns is important in both technology and fundamental science. In many technological processes, the naturally occurring flow patterns may not be the optimal ones. By controlling the flow, one may be able to optimize the process. The ability to stabilize otherwise non-stable states may also assist one in gaining deeper insights into the dynamics of flows. Since fluid flow phenomena are highly nonlinear and possess many degrees of freedom, the flow control problem is far from trivial.

In prior experimental and theoretical investigations, Singer, Wang & Bau (1991), Singer & Bau (1991), Wang, Singer & Bau (1992), Yuen & Bau (1996) and Yuen (1997) used various linear and nonlinear control strategies to alter the bifurcation structure of the convective motion in a thermal convection loop heated from below and cooled from above. For example, with the aid of a controller, they were able to delay the transition from a no-motion to a motion state, laminarize the naturally occurring chaotic motion in the loop, stabilize otherwise non-stable periodic orbits embedded in the chaotic attractor, render subcritical bifurcations supercritical, and induce chaos under conditions in which the flow normally would be laminar. In the case of the thermal convection loop, they were able to control the relatively low-dimension temporally complex flows using a single actuator. The objective of this paper is to determine whether systems with many spatial degrees of freedom and whose control requires multiple sensors and actuators can also be successfully controlled. To this end, we investigate the feasibility of delaying the transition from the no-motion (pure

† Current address: Aeroquip Corporation, Corporate Technology, 2323 Green Road, Ann Arbor, MI 48105-1530, USA.

‡ All correspondence should be directed to this author: e-mail address bau@seas.upenn.edu.

conduction) to the motion state in the Rayleigh–Bénard problem of a fluid layer heated from below and cooled from above. We have chosen this problem for study because the uncontrolled problem has been extensively studied and the phenomena observed are relatively well understood. The Rayleigh–Bénard problem is also of technological importance since it serves as a paradigm for many material processing applications.

A considerable amount of work has been devoted to delaying the onset of Rayleigh–Bénard convection. Most of these attempts included the use of predetermined (open loop control), time-periodic modulation of the temperature difference across the layer (for lucid reviews, see Davis 1976 and Donnelly 1990). Unfortunately, this technique provides only marginal stabilization. Moreover, periodic modulation may lead to a subcritical bifurcation (Roppo, Davis & Rosenblat 1984), thereby causing the no-motion state to be stable only for small disturbances. Kelly (1992) and Kelly & Hu (1993) proposed delaying the onset of cellular convection by causing the fluid in the layer to oscillate slowly about a zero mean with two out-of-phase horizontal velocity components. In contrast, our objective is to maintain a state of complete rest.

In theoretical studies, Tang & Bau (1993*a*, *b*, 1994, 1995) have shown that with the aid of a feedback controller the critical Rayleigh number for the onset of convection in an infinite horizontal fluid layer can be increased by almost an order of magnitude. Using the control strategies of Tang & Bau, Howle (1997) demonstrated experimentally that feedback control can be used to reduce the intensity of two-dimensional convection in a slender box. In the present investigation, we test the feasibility of applying our control ideas in the three-dimensional setting of an upright circular cylinder.

## 2. Experimental apparatus

We conducted our experiments in an upright circular cylinder made of Plexiglas. A cross-section of the experimental apparatus is depicted in figure 1. Three rings (labelled 2, 3, and 4) were stacked to form a test chamber (1) with both an inner diameter and a height of 3.5 cm. The middle ring (3) carried the diode sensors (figure 3). The upper boundary (5) of the test cell was made of a high-thermal-conductivity sapphire plate. Cooling water, at 23 °C, was supplied by a constant-temperature bath and circulated in the cooling chamber (6) located above the sapphire plate. The top of the cooling chamber was capped with a glass plate (7) covered by Plexiglas ring (8). The bottom of the test cell consisted of a silicon wafer (9) supported on a Plexiglas ring equipped with supporting chordal beams (10). The heater support ring (10) was positioned on top of another ring (11) which provided space for the electrical connections needed to supply power to the many heaters installed on the silicon wafer. The entire apparatus sat on top of a flat plate (12). Four bolts (13) positioned at the corners of the plate (12) facilitated the levelling of the apparatus and assured that its axis was parallel to the gravity vector. The various rings were connected with the aid of alignment pins (14) and screws (15). O-rings (16) were inserted between the various rings in figure 1 to prevent leaks. The test chamber was equipped with venting holes (not shown) to facilitate thermal expansion of the test fluid.

The thermal actuators (heaters) were installed on the underside of the wafer (labelled 9 in figure 1), and they supplied the nominal heating needed to drive the buoyant flow as well as the means for controlling that flow. Figure 2 depicts schematically the silicon wafer and the location of the individual heaters. The heater numbers in figure 2 are identical to the numbers identifying the diodes located directly above the heaters at the

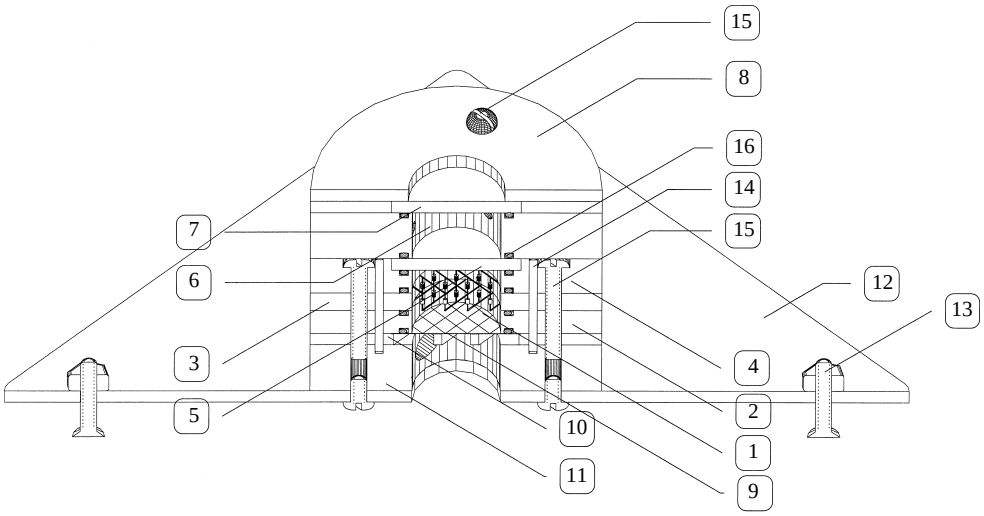


FIGURE 1. A schematic description of a cross-section of the experimental apparatus: (1) the test chamber; (2) lower ring forming the test chamber; (3) a diode-sensor carrying ring; (4) the top ring forming the upper part of the test chamber; (5) sapphire disk; (6) cooling chamber; (7) glass cover disk; (8) Plexiglas ring cover; (9) silicon wafer containing heaters; (10) heater support ring; (11) bottom ring providing room for electrical connections; (12) base plate; (13) levelling bolts; (14) alignment pins; (15) tightening screws; and (16) O-rings.

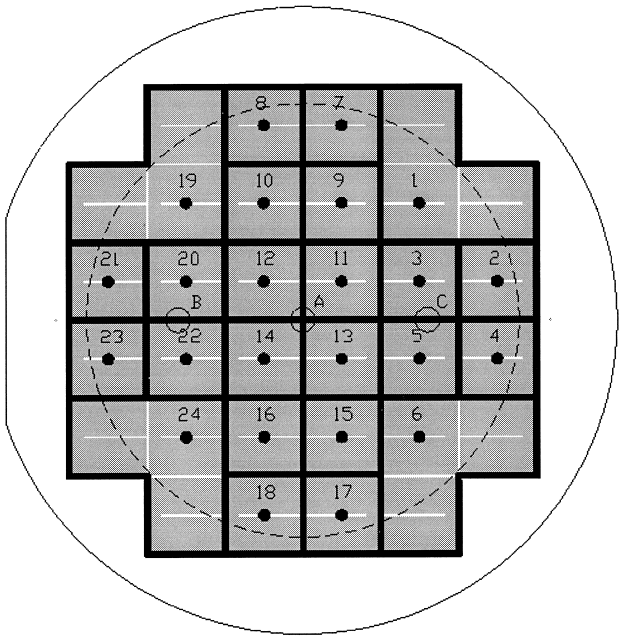


FIGURE 2. A schematic description of the heating surface. The thick lines describe schematically the boundaries of the individual heaters. The dashed circle describes the inner circumference of the test cell. The numbers on the heaters correspond to the numbers identifying the diodes located directly above the heaters. The three circles describe the location of the three bottom thermocouples.

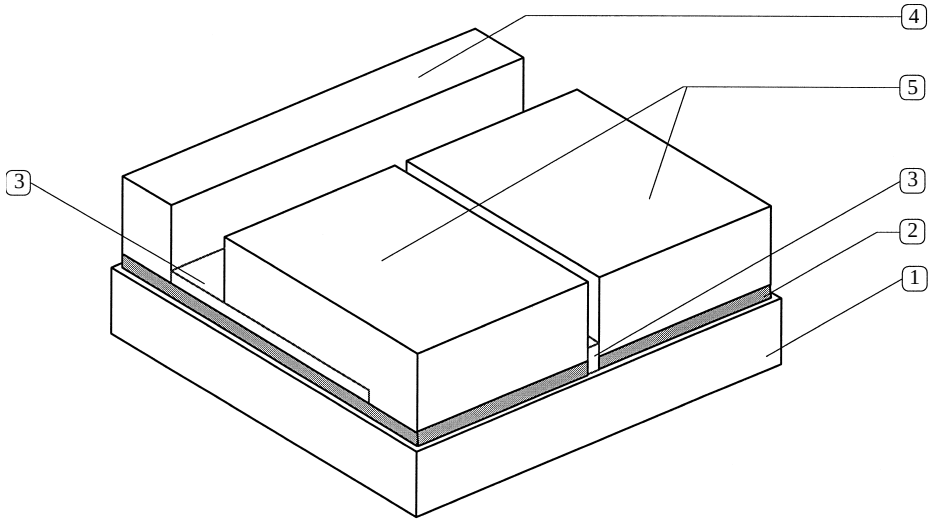


FIGURE 3. Three-dimensional depiction (not drawn to scale) of a single heater: (1) $SiO_2$ coated silicon substrate; (2) nichrome; (3) silicon nitride; (4) gold electrode connecting the two slices of the heater; and (5) gold bonding pads.

cell midplane. The dashed circle shows the location of the inner circumference of the test cell. The wafer contained a total of 32 heaters. The four groups of three heaters located at the corners of the heater array operated in series. Consequently, 20 heaters and four groups of three heaters each were individually controlled. In order to minimize the bottom-plate area consumed by lead wires and electrical connections, we used microfabrication technology to manufacture the heaters. Although we fabricated both rectangular heaters and heaters shaped like circular sectors, only rectangular heaters were used in the experiments reported here. This was done to minimize variations in the heaters' electrical resistances.

Figure 3 depicts schematically the structure of a single heater. The fabrication technique is described briefly below. On a double polished 300 μm thick (110) silicon wafer (item 1 in figure 3 depicts a piece of the wafer), we oxidized a 1 μm thick layer to serve as an electrically insulating layer. On top of the oxide layer, we deposited a 1000 Å thick nichrome layer (2). The nichrome was etched to form 32 individual heaters 6.1 mm × 6.1 mm each. Each heater consisted of two 3 mm × 6.1 mm slices separated by a 100 μm thick gap. This separation was done to increase the heater's electrical resistance. Later on, the two slices were connected at one side by a gold electrode (4) and the other side of each slice was connected to a gold pad (5) which accommodated lead wires. The distance between adjacent heaters was also 100 μm.

On top of the nichrome, we sputtered a 1 μm layer of insulating silicon nitride (3). Using plasma etch, we opened windows in the silicon nitride to facilitate electrical connections. On top of the silicon nitride, we sputtered a 1000 Å thick gold layer. In order to minimize parasite electrical resistance, the thickness of the gold leads and pads was increased to 1 μm by electroplating. This gold layer was then wet etched to form electrodes (4), leads, and bonding pads (5). The gold electrodes assured uniform distribution of current in the heaters. The bonding pads allowed ample space for soldering lead wires without interfering with the heaters themselves. The lead wires to the actuators were positioned outside the test chamber.

One of the bonding pads of each heater was grounded. The other side of each heater

was connected to a programmable power supply made of operational amplifiers (APEX PA01) and digital to analog converters (DAC, Analog Devices, AD558JN). The DACs retained their signals between updates. The 24 power supplies were controlled by digital I/O lines and a personal computer. To minimize the number of I/O lines needed, demultiplexer chips were used to select any of the power supplies. The details of the electronic connections and instruments are lengthy and are described in detail in Tang (1996).

Mircofabrication technology allows us to manufacture much smaller actuators (heaters) than the ones used in our experiment. The space needed to connect the actuators to external devices and the cost of power supplies limited, however, the number of actuators which we were able to use.

The voltage of the power amplifiers was controlled with an 8-bit resolution. This resulted in a relatively crude power resolution. For example, the power could be incremented only in steps of 2.7 mW/heater around the nominal power setting of 10 m W/heater and 4.6 mW/heater around the nominal power setting of 50 mW/heater. Although the relatively high thermal conductivity of the silicon wafer helped smooth power variations among the heater, the crude power control may have caused some non-uniformity in the bottom plate's heat distribution.

In the course of the initial experiments, we observed that the heaters' resistance decreased with time by as much as 25%. This ageing process may have been caused by the annealing of the nichrome or the diffusion of gold into the nichrome, and it became insignificant after a few hours of operation. The average resistance of the aged heaters was 27 $\Omega$ with a 2 $\Omega$ standard deviation. The voltage supplied to each heater was computed so as to obtain the desired power while accounting for differences in individual heater's resistance.

Unfortunately, the very many lead wires which were needed to control the individual heaters and the wafer supports provided a thermal path for heat losses. Additional power losses occurred by radial conduction through the silicon wafer and into the test cell's sidewalls and the supporting structure. Therefore, a significant fraction of the power supplied to the heaters was dissipated to the environment. This precluded us from using the power input as a measure of the heat transfer through the fluid layer. Likewise, we were not able to determine the Nusselt number and the heat-flux-based Rayleigh number. Additionally, due to the relatively high flow rate of the cooling water that was needed to maintain a uniform top temperature and because of the thermal interaction of the cooling chamber with the environment, we were not able to use the flow rate and the increase in the cooling water's bulk temperature to compute the amount of heat transported through the test cell. This paper's main objective, however, is to compare the flow patterns in the controlled and uncontrolled states. Such a comparison can be accomplished without measuring the heat transfer.

Although in applications it would be desirable to use non-intrusive sensors such as sensors embedded in the surface of the silicon wafer that is in contact with the fluid, our preliminary theory (Tang 1996) suggested that a more effective location of the sensors is at about the fluid layer's midheight. Since, in this exploratory study, we wish to demonstrate experimentally that it is possible to control flow patterns, we embedded the sensors at the fluid's midheight. In the future, we hope to develop other control strategies that would allow us to position the sensors at less intrusive locations.

We have selected diodes to serve as temperature sensors because of their high sensitivity and because they allow only unidirectional current flow, which in turn permitted a significant reduction in the number of lead wires and multiplexer channels compared to what would have been required if one were to use other sensing devices.

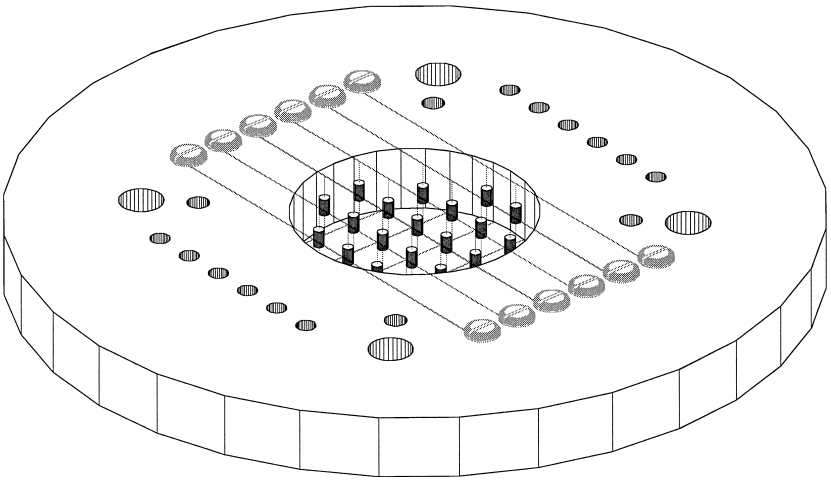

FIGURE 4. A three-dimensional depiction of the diode carrying ring (item 3 in figure 1) and the diode sensors.

Twenty-four diodes were connected between two sets of six intersecting wires stretched on the two sides of a Plexiglas ring (figure 4 and item 3 in figure 1). We denote one set of parallel wires (i.e. the wires on the top of the disk in figure 4) with the letters A, B, …, and the other set (i.e. the wires on the bottom side of the disk in figure 4, not visible) with the numbers 1, 2, …. For example, the temperature sensed by diode C4 can be read by applying a constant current to wires C and 4 and measuring the forward-biased voltage across these wires. In general, to measure $n^2$ diodes, one would need only two sets of $n$ intersecting wires and $2n$ electromagnetic relays. In our set-up, the $2n = 12$ wires were connected to two electromagnetic relay boards (SC-2062, National Instruments). The relays were controlled by digital signals from a multi-function data acquisition board (AT-MIO-16DE10, National Instruments) and the measured voltage was transmitted to the same data acquisition board.

The glass-encapsulated silicon diodes (1 mm diameter and 2 mm length) were individually calibrated in a constant-temperature bath of silicon oil to facilitate temperature measurement with $\pm 0.1$ °C precision. In the range of temperatures of interest, the voltage drop of the forward-biased diodes was nearly a linear function of the temperature. All the calibration curves had similar slopes but different levels. To obtain a temperature reading, the diode voltage was averaged for half a second at a scanning rate of 1000 readings/s. The diodes were positioned at the cylinder's midheight with a precision of $\pm 1$ mm so that there was one diode above each of the individually controlled heaters. The horizontal location of the different diodes is depicted in figure 2.

The temperatures of the heated surface, cooling water, water bath, and the ambient were measured with type T 36AWG thermocouples. All the thermocouples were individually calibrated to yield a precision of $\pm 0.5$ °C. Three thermocouples were glued on the back side of the silicon wafer with conducting epoxy. The location of these thermocouples is indicated by the circles A, B, and C in figure 2. We used the average reading of these three thermocouples as a rough indicator of the bottom plate temperature. Two thermocouples measured the cooling water temperature. These thermocouple measurements provided an estimate for the sapphire plate temperature. One thermocouple monitored the cooling bath temperature and another the ambient temperature. All the thermocouples were connected to a Hewlett-Packard data

acquisition system (HP 3497A) and a digital voltmeter (HP 3456A). The measurements were controlled by a personal computer via a GP-IB interface card (AT-GPIB/TNT, National Instruments).

During the experiments, the apparatus was well insulated to minimize thermal interaction with the environment. Two sets of experiments were conducted using Dow Corning silicon fluid 200 (5000 cS). In the first set of experiments, the controller was not active and uniform power was supplied to all the heaters. In the second set of experiments, the controller was active and the heaters' power was varied according to a pre-determined rule. In both the uncontrolled and controlled experiments, the midheight temperatures, the bottom temperatures, the cooling water temperature, the ambient temperature, and the power of each individual heater were monitored as functions of time.

Automated data collection and the control functions were facilitated through the use of a personal computer running Labview for Windows. In the controlled experiments, the heaters' power was updated about every 50 s. The time constant of the conduction was estimated to be about 2.7 h. In the presence of convection, the time constant was smaller. This time constant was a function of the convection's intensity, and in all cases, it consisted of many minutes.

## 3. The uncontrolled case

We first carried out measurements in the absence of a controller. The purpose of these experiments was to provide a reference state against which the controlled flow would be compared. These experiments are also of interest in themselves since they provide information on Rayleigh–Bénard convection in an upright circular cylinder. The power was varied from 0 W/heater to 0.05 W/heater (up to a total power input, $P_{max} = 1.6$ W). In the range of powers considered here, in all the uncontrolled cases, after initial transients died out a steady time-independent state was established. All the results reported in this section were obtained after a steady state was established. We defined the state to be steady once the midheight temperature varied less than 0.05 °C over a period of 5 h.

Figure 5 depicts the steady-state temperature readings of diodes 1, 15, 16, and 19 as functions of the average heater power. For low power settings ($p < p_c \sim 32 \pm 1$ MW/heater), the midplane temperatures increased nearly linearly as the heater power increased. When $p < p_c$, each diode temperature could be correlated by a straight line (solid line in figure 5) of the form

$$T_{i,c} = b_i + a_i\, p_i, \tag{1}$$

where $T_i$ is the temperature reading of the $i$th diode, the subscript $c$ denotes a correlated value, $p_i$ is the power supplied to the $i$th heater, and $a_i$ and $b_i$ are constants. Different diodes had different constants. Ignoring the temperature dependence of the thermophysical properties, equation (1) is consistent with conduction-dominated heat transmission. The solid line in figure 5 does not intersect the origin since the cooling water temperature ($T_0$) differs from the ambient temperature.

Figure 5 suggests that when $p < p_c$, heat was transported predominantly by conduction in the liquid layer. When $p > p_c$, significant deviations from this linear behaviour were observed. In other words, at $p \sim p_c$ a transition occurred from a conduction-dominated state to a state in which convection plays a significant role. When $p > p_c$, diodes recording temperatures above (below) the straight line were submerged in ascending (descending) flow.

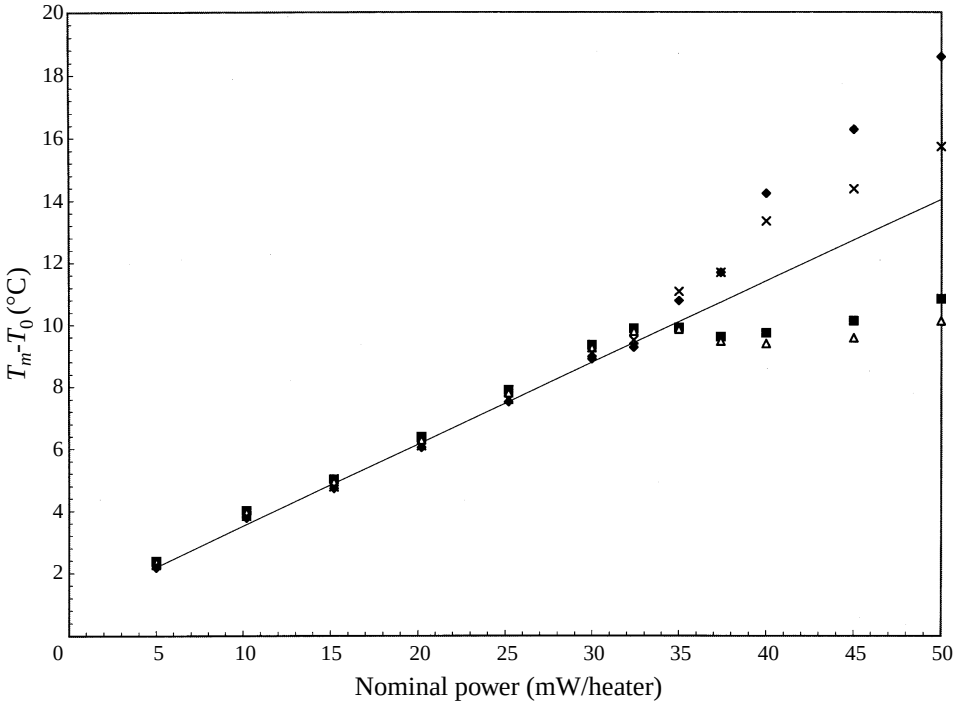


FIGURE 5. The temperatures, at various locations at the cylinder midheight, as read by diodes 1 (◆), 15 (■), 16 (△), and 19 (×), are depicted as functions of the average heater power. The location of the various diodes is given in figure 2. The solid line is a linear correlation of the low-power ($p < 30$ mW/heater) data.

Table 1($a$) lists the relative temperature readings of the various diodes, $\theta_i = (T_i - T_0)/\Delta\bar{T}_{BT}$, when $p_i = 5$ mW/heater. Here, $\Delta\bar{T}_{BT}$ is the difference between the average bottom temperature as measured by three thermocouples and the cooling water temperature, $T_0$. Not all the diodes recorded exactly the same temperature, as they should have for a perfectly conductive state. The small temperature differences between the various diode readings were possibly a result of height differences in the diode locations (which we estimate to be within $\pm 2.8\,\%$), thermal interaction with the surroundings, and the possible presence of weak convection due to inevitable imperfections in the experimental apparatus.

When $p > p_c$, the diode temperatures no longer depended linearly on the power input. The relative diode temperatures, $\theta_i$, for $p_i = 50$ MW/heater are recorded in table 1($b$). Note that the temperatures in the upper half of the cylinder cross-section are significantly higher than those in the lower half. This temperature distribution is consistent with a single convective cell. The cylinder can be viewed as divided by an imaginary vertical plane into two halves with fluid ascending in one half and descending in the other half. For a cylinder with an aspect ratio (radius/height) of 0.5, this flow pattern is similar to experimental observations and numerical simulations made by other researchers (i.e. Müller, Neumman & Weber 1984; Neumman 1990) as well as with our own numerical simulations (Tang 1996). When repeating the experiments, we always observed a single cell structure, although the orientation of the cell varied from one experiment to another.

To eliminate the uncertainty due to possible misalignment of the diodes, instead of relying on the actual diode measurement, we used the difference between the measured

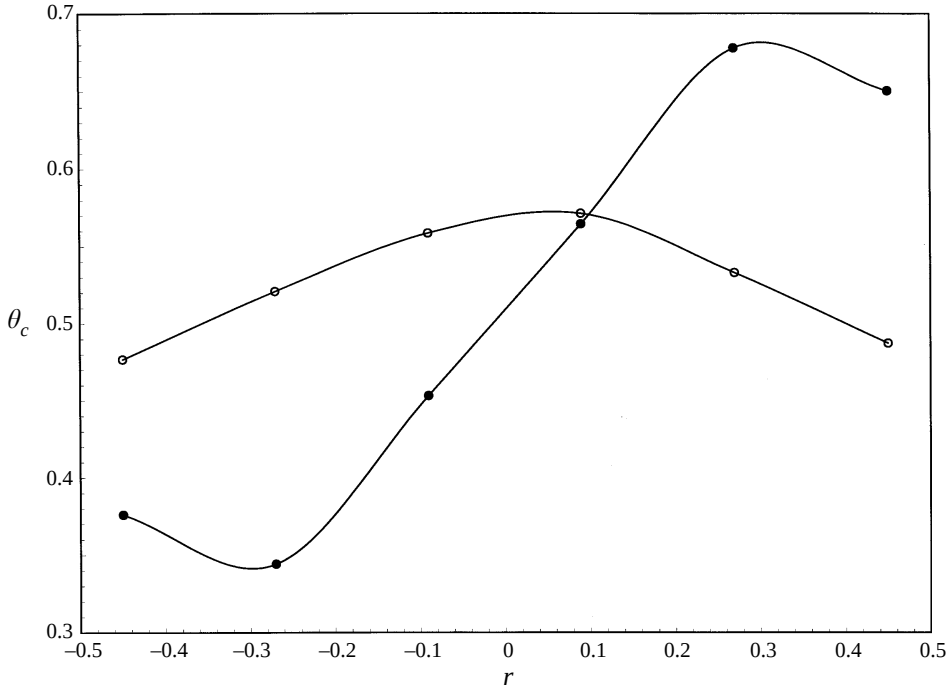


FIGURE 6. The midplane temperature as a function of the radial location along a diameter on which the maximum and minimum temperatures were observed. The heater power was 50 mW/heater. Solid and hollow circles represent experiments without ($k_p = 0$) and with a controller ($k_p = 0.1$ W $K^{-1}$).

| | | 1 | 2 | 3 | 4 | 5 | 6 |
|---|---|---|---|---|---|---|---|
| (*a*) | 1 | — | — | 0.49 | 0.51 | — | — |
| | 2 | — | 0.48 | 0.45 | 0.52 | 0.50 | — |
| | 3 | 0.52 | 0.51 | 0.54 | 0.52 | 0.52 | 0.46 |
| | 4 | 0.50 | 0.52 | 0.53 | 0.52 | 0.51 | 0.49 |
| | 5 | — | 0.51 | 0.53 | 0.53 | 0.51 | — |
| | 6 | — | — | 0.50 | 0.48 | — | — |
| (*b*) | 1 | — | — | 0.64 | 0.62 | — | — |
| | 2 | — | 0.65 | 0.70 | 0.66 | 0.55 | — |
| | 3 | 0.54 | 0.57 | 0.60 | 0.55 | 0.49 | 0.43 |
| | 4 | 0.47 | 0.48 | 0.48 | 0.43 | 0.40 | 0.39 |
| | 5 | — | 0.41 | 0.38 | 0.36 | 0.35 | — |
| | 6 | — | — | 0.38 | 0.37 | — | — |
| (*c*) | 1 | — | — | 0.46 | 0.48 | — | — |
| | 2 | — | 0.46 | 0.50 | 0.51 | 0.49 | — |
| | 3 | 0.45 | 0.47 | 0.54 | 0.54 | 0.52 | 0.47 |
| | 4 | 0.45 | 0.49 | 0.53 | 0.56 | 0.52 | 0.48 |
| | 5 | — | 0.48 | 0.52 | 0.52 | 0.49 | — |
| | 6 | — | — | 0.48 | 0.49 | — | — |

TABLE 1. The relative midplane temperatures when (*a*) the power input is 5 mW/heater and there is no controller; (*b*) the power input is 50 mW/heater and there is no controller; (*c*) the power input is 40 mW/heater and a controller with a gain of 32 mW $K^{-1}$ is active. The horizontal location of the diodes is given in figure 2.

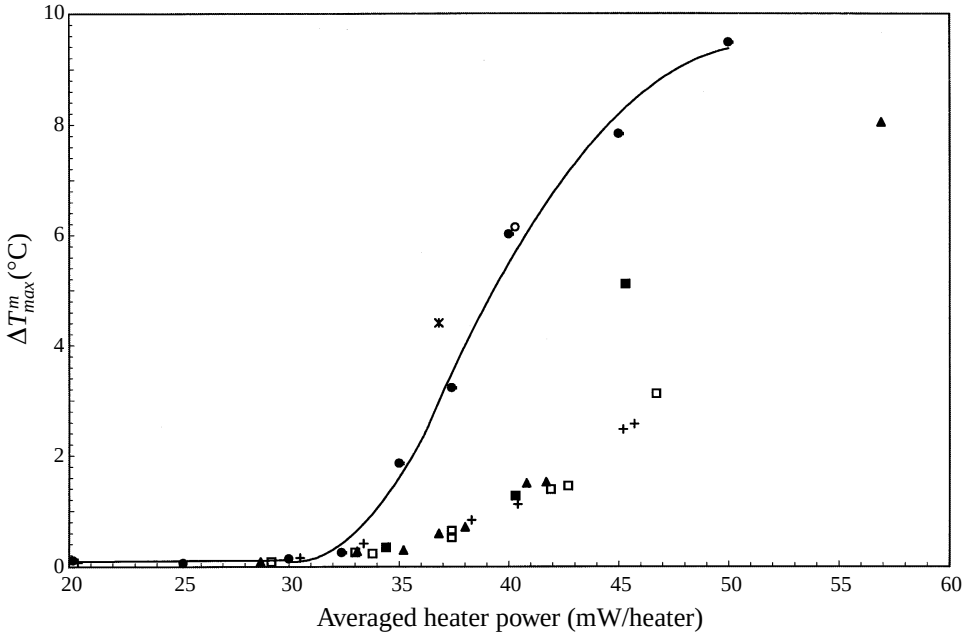


FIGURE 7. The time-averaged maximum midplane temperature difference, $\Delta T^m_{max}$ as a function of the time-averaged average power input to the heaters and various control gains: $k_p = 0$, (no control, ●), 32 (■), 70 (▲), 100 (□), and 200 (+) mW K$^{-1}$. The circle represents data from experiments in which the controller was turned-off and the power distribution was 'frozen' at the time-averaged power levels measured in the controlled experiments with $k_p = 32$ mW K$^{-1}$; * represents data when $k_p = 70$ mW K$^{-1}$.

value and the extrapolated value given by equation (1). For the relatively small supercritical powers of our experiments, we used the corrected value of the diodes maximum temperature difference, $\Delta T^m_{max_i} \equiv \max_i(T_i - T_{i,c}) - \min_i(T_i - T_{i,c})$, as a measure for the intensity of the convection.

Numerical simulations (Tang 1996) suggest that, in the range $1 < p/p_c < 1.6$, $\Delta T^m_{max}$ increases monotonically as a function of $p$. When $p$ is further increased, $\Delta T^m_{max}$ does not vary significantly and eventually it declines. Since all our experiments were carried out in the region $p/p_c < 1.6$, $\Delta T^m_{max}$ served as an adequate measure of the convection intensity.

Figure 6 depicts the temperature distribution along a 'diameter' of the cylinder on which the maximum and the minimum temperatures were detected when $p_i = 50$ mW/heater. The curve was constructed by recording the temperatures registered by the diodes that were closest to the selected diameter. The figure depicts $\theta_{i,c} = (T_{i,c} - T_0)/\Delta \bar{T}_{BT}$ as a function of the normalized radius $r$. Here, $k_p$ denotes the controller gain, and $k_p = 0$ (solid circles) signifies that the controller was not active. The radius was normalized with the cell height. The temperature distribution depicted in figure 6 is consistent with a single-cell flow pattern.

Figure 7 ($k_p = 0$, solid circles) depicts $\Delta T^m_{max}$ as a function of the heater power input. Like figure 5, figure 7 suggests that at $p \sim p_c = 30$ mW/heater, convection gains importance. Figure 8 ($k_p = 0$, solid circles) depicts the maximum corrected diode temperature difference, $\Delta T^m_{max}$, as a function of the average bottom–top temperature difference, $\Delta \bar{T}_{BT}$. The figure indicates that in the uncontrolled case, the transition from the conduction-dominated state to a state in which convection plays a significant

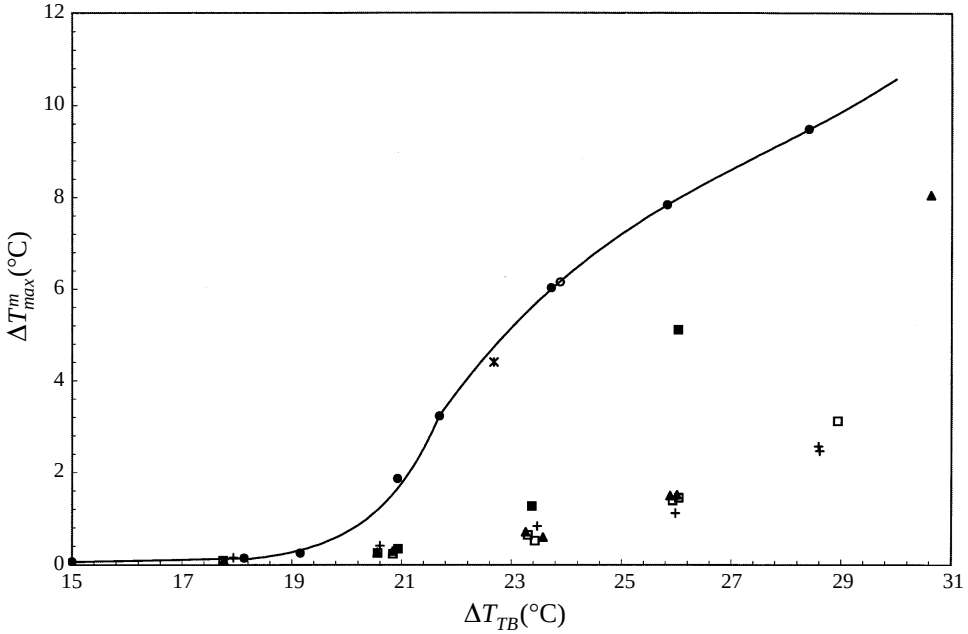


FIGURE 8. The time-averaged maximum midplane temperature difference, $\Delta T^m_{max}$ as a function of the time-averaged average bottom–top temperature difference, $\Delta T_{BT}$, and various control gains: $k_p = 0$ (no control, ●), 32 (■), 70 (▲), 100 (□), and 200 (+) mW K$^{-1}$. The open circle represents data from experiments in which the controller was turned off and the power distribution was 'frozen' at the time-averaged power levels measured in the controlled experiments with $k_p = 32$ mW K$^{-1}$; * represents data when $k_p = 70$ mW K$^{-1}$.

role occurs at $\Delta\bar{T}_{BT,c} \sim 19$ °C. Both figures 7 and 8 exhibit a smooth transition from the predominantly conductive to the convective state. This suggests that the bifurcation is not perfect and that convective currents are always present.

Since the thermophysical properties of the test fluid and their temperature dependence are not reliably known, we could obtain only a rough estimate for the critical Rayleigh number at the onset of convection. Based on the Dow Corning 200 Fluid Data sheet, the temperature difference, $\Delta\bar{T}_{BT,c} \sim 19$ °C, corresponds to a Rayleigh number based on bottom–top temperature difference based, $Ra = (g\beta\Delta\bar{T}_{TB}H^3)/(\alpha\nu)$, of about 12780. This is significantly larger than the theoretically estimated value of $\sim 7500$. The discrepancy between the theoretical and experimental values can be attributed mostly to the uncertainty in the fluid thermophysical properties and in a smaller part to the presence of the diode array that added resistance to the flow and provided a stabilizing effect. Since in our study we compare the performance of the controlled and uncontrolled systems, accurate knowledge of the critical Rayleigh number is not essential. In the above, $g$ is the gravitational acceleration, $\beta \sim 9.6 \times 10^{-4}$ K$^{-1}$ is the thermal expansion coefficient, $H = 3.5$ cm is the height of the test cell, and $\alpha \sim 1.2 \times 10^{-7}$ m$^2$ s$^{-1}$ and $\nu \sim 5 \times 10^{-3}$ m$^2$ s$^{-1}$ are the thermal diffusivity and the kinematic viscosity of the fluid.

Figure 9 ($k_p = 0$, solid diamonds) depicts the average bottom–top temperature difference, $\Delta\bar{T}_{BT}$, as a function of the heater power $p_i$. The uncontrolled case is represented by a solid line when $p < p_c$ and by a dashed line when $p > p_c$. Note the change in the slope of the curve at $p_i \sim p_{i,c}$ and $\Delta\bar{T}_{BT} \sim \Delta\bar{T}_{BT,c}$ (the intersection between the solid and dashed lines). This is consistent with convection gaining

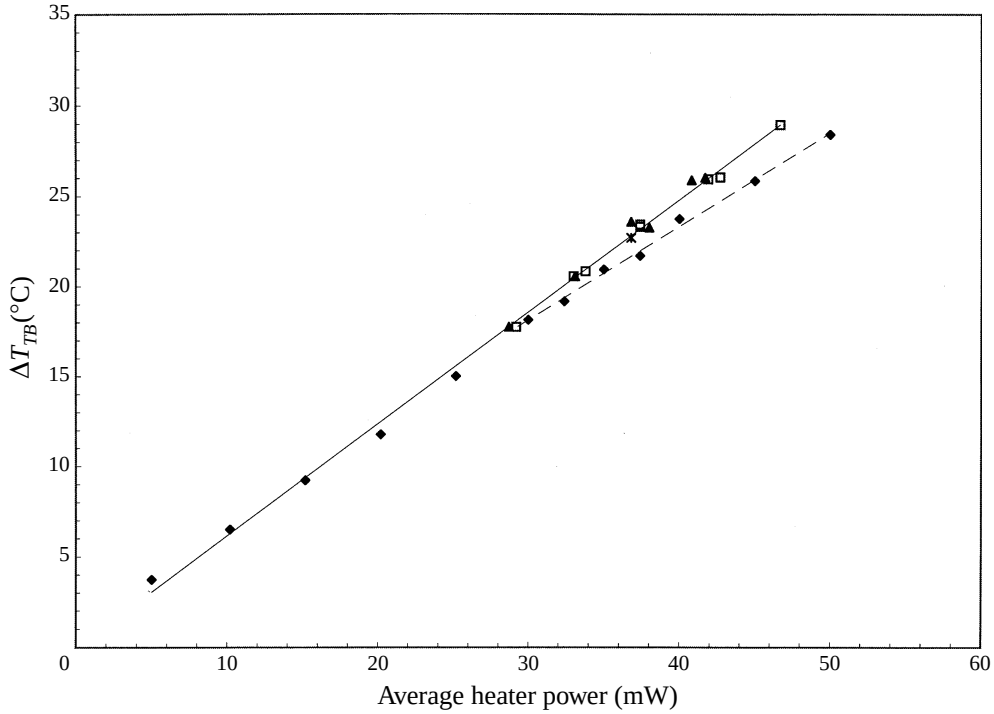


FIGURE 9. The time-averaged bottom-top temperature difference, $\Delta T_{BT}$ as a function of the time-averaged average power input to the heaters and various control gains: $k_p = 0$ (no control, ◆), 70 (▲), and 100 (□) mW K$^{-1}$. The circle represents data from experiments in which the controller was turned-off and the power distribution was 'frozen' at the time-averaged power levels measured in the controlled experiments with $k_p = 32$ mW K$^{-1}$; * represents data when $k_p = 70$ mW K$^{-1}$.

importance at $p_i \sim p_{i,c}$. The presence of convection reduces the thermal resistance of the fluid layer. Therefore, when convection is present, a smaller $\Delta \bar{T}_{BT}$ is needed to transfer a similar amount of heat than when convection is absent.

In the conductive regime, we expect the bottom temperature to be almost uniform. When convection sets in, the temperature at the location of the ascending flow is expected to be higher than that at the location of the descending flow. Figure 10 ($k_p = 0$, solid diamonds and solid line) depicts the maximum relative difference in the bottom temperature, $\Delta T_B = \max_i(T_{B,i}) - \min_i(T_{B,i})$, as a function of the average heater power. In contrast to expectations, in the uncontrolled case $\Delta T_B$ increases nearly linearly as the power increases. This behaviour may be due to differences in the thermal resistance associated with the mounting of the various thermocouples, radial conduction in the silicon wafer and heat losses through the bottom plate perimeter, and the presence of weak convection in the apparatus when $p < p_c$.

Thus far we have described our measurements when the bottom heat flux was uniform, pre-determined, and time-independent. In the next section, we describe the measurements when the heater power was allowed to vary in proportion to the midheight temperature deviations from their no-motion-state values. We will compare the data obtained in the controlled case with that of the uncontrolled case.

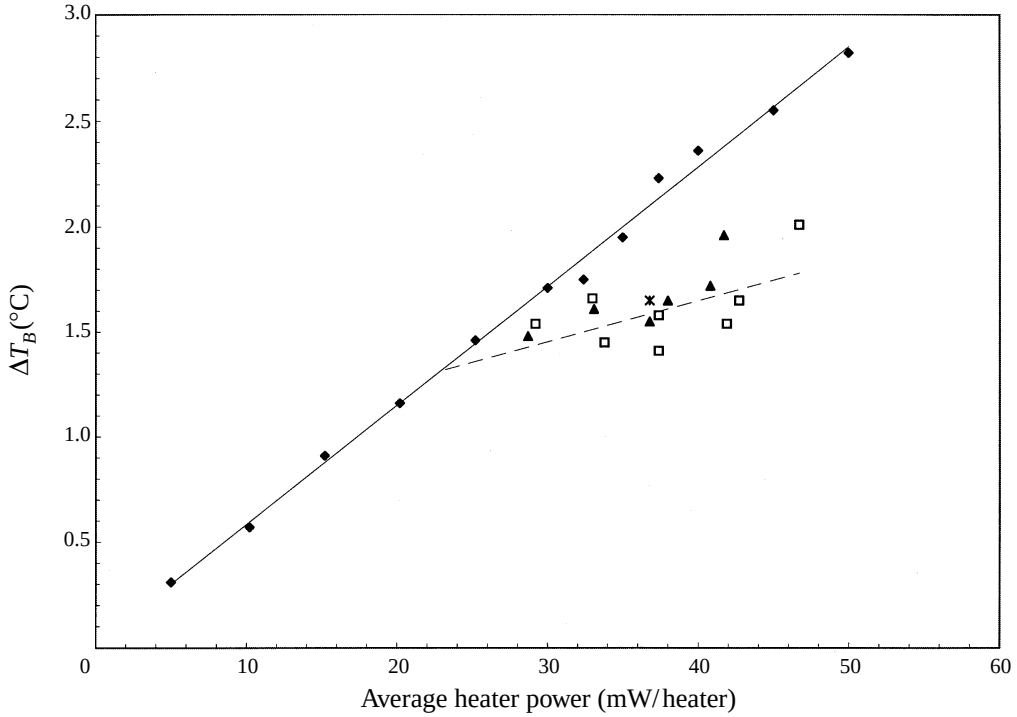


FIGURE 10. The time-averaged maximum bottom temperature difference, $\Delta T_B$ as a function of the time-averaged average power input to the heaters and various control gains: $k_p = 0$ (no control, ◆), 70 (▲), and 100 (□) mW K$^{-1}$. The circle represents data from experiments in which the controller was turned-off and the power distribution was 'frozen' at the time-averaged power levels measured in the controlled experiments with $k_p = 32$ mW K$^{-1}$; * represents data when $k_p = 70$ mW K$^{-1}$.

## 4. The controlled case

In the controlled experiments, the diodes were continuously scanned to obtain the midheight temperature, $T_i$. Once every 50 s, the heater power was modified according to the proportional feedback rule,

$$p_{i,j} = p_0 - k_p(T_{i,j} - T_{i,c}), \tag{2}$$

where $p_{i,j}$ is the power provided to heater $i$ at the time interval from $j$ to $j+1$; $p_0$ is the nominal (desired) power; $T_{i,j}$ is the temperature reading of diode $i$ at time $j$; $k_p$ is the proportional controller gain; and $T_{i,c}$ is the desired, extrapolated (conductive) temperature corresponding to power $p_{i,0}$ and computed from equation (1). The control strategy described by equation (2) is not necessarily optimal. One can envision more complicated control strategies such as having all the sensors communicating with all the actuators. For example, instead of using a scalar gain, one could use a gain tensor, $k_{i,m}$, i.e.

$$p_{i,j} = p_0 - \sum_m k_{i,m}(T_{m,j} - T_{m,c}), \tag{3}$$

which renders the power input to each heater a function of all the diode readings. Since we do not have yet the theoretical justification for using such a control strategy (3), in all our experiments we used the control strategy given by equation (2). In prior theoretical investigations, Tang & Bau (1994) have shown this control strategy to be effective.

As a result of unavoidable fluctuations, which are always present in any physical

system, the measured temperatures, $T_i$, oscillated slightly as a function of time. Subsequently, the control rule caused timewise oscillations in the power input. As long as the control gain was small, these oscillations had a relatively small amplitude. For example, when the nominal power was 40 mW/heater and the controller gain 32 mW $K^{-1}$, the amplitude of the temperature oscillations at midheight and at the bottom were, respectively, of the order of 0.01 °C and 0.1 °C.

In this section, unless we state otherwise, all reported results are time-averaged quantities. For example, $p_i = (1/N_T)\Sigma_{j=1}^{N_T} p_{i,j}$, where $p_i$ is the time-averaged power input to the $i$th heater and $N_T$ is the number of uniform time intervals during the experiment. In most cases, the averaging process was carried out for as long as three hours. All other measured quantities were time averaged in a similar fashion.

In the first set of experiments, with the controller active, we increased gradually the heating rate and recorded the temperature fields and the time-averaged power consumption of each heater.

Figure 7 depicts the corrected time-averaged maximum midplane temperature difference, $\Delta T^m_{max}$, as a function of the time-averaged average power input to the heaters, $\bar{p} = (1/N_H)\Sigma_{i=1}^{N_H}(p_i)$, and various control gains, $k_p = 0$ (no control), 32, 70, 100, and 200 MW $K^{-1}$. Here, $N_H$ represents the number of heaters. Figure 7 illustrates that in the presence of the controller, the maximum midheight temperature difference is significantly lower than in the controller's absence. The onset of 'significant' convection has been delayed from an average power input of $\sim$ 30 mW/heater in the absence of a controller to about 37 mW/heater in the presence of a controller. Once convection started, $\Delta T^m_{max}$ in the controlled case was much smaller than in the uncontrolled case. For example, at average heater power of 40 mW/heater and a control gain 32 mW $K^{-1}$, $\Delta T^m_{max} \sim 1.3$ °C. This value should be contrasted with $\Delta T^m_{max} \sim 6$ °C for the same power input in the absence of a controller. As the average heater power increased, it was necessary to increase the controller gain in order to further suppress the convection.

Figure 8 depicts $\Delta T^m_{max}$ as a function of the time-averaged average bottom–top temperature difference, $\Delta \bar{T}_{BT}$, and various controller gains, $k_p = 0$ no control), 32, 70, 100, and 200 mW $K^{-1}$. Figure 8 is consistent with figure 7. For similar bottom–top temperature differences ($\Delta \bar{T}_{BT}$), $\Delta T^m_{max}$ is significantly smaller in the presence of the controller than in its absence. The onset of significant convection has shifted from $\Delta T_{BT} \sim 19$ °C in the absence of the controller to $\Delta T_{TB} > 23$ °C when the controller was active.

In the presence of the controller, the flow patterns were different than in its absence. Table 1($c$) lists the relative diode temperatures for the average heater power $p_i = 40$ mW/heater and controller gain of 32 mW $K^{-1}$. This table should be compared with table 1($b$) (no control). The temperature variations in table 1($c$) are significantly smaller than in table 1($b$). Note that the temperature maximum has shifted from the side of the cylinder (table 1$b$) to the cylinder's centre (table 1$c$). This temperature distribution is consistent with heat losses through the vertical walls and weak axisymmetric convection with flow ascending at the cylinder centre and descending next to the cylinder wall.

The temperature distribution along the diameter of the cylinder on which maximum and minimum temperatures were detected when $p_i = 50$ mW/heater and $k_p = 0.1$ W $K^{-1}$ is depicted in figure 6. Note that in the controlled case (open circles), the temperature distribution is much flatter than in the uncontrolled case (solid circles).

In contrast to expectations, when the controller was active, the time-averaged power supplied to the various heaters was not uniform. Table 2 documents the power (mW)

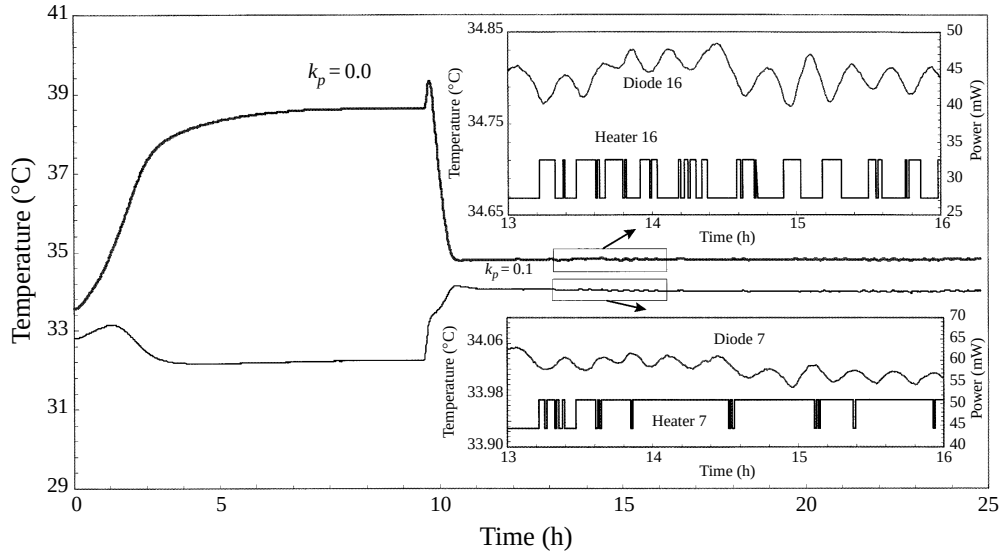


FIGURE 11. The temperatures as measured by diodes 7 (light line) and 16 (heavy line) as functions of time. The power is gradually increased until steady-state convection begins while the controller is off. At time $t = 9.54$ h, the controller with a gain 0.1 W K$^{-1}$ was turned on and remained active. Magnified temperatures and powers of two diode-actuator pairs are depicted as functions of time in the inserts.

| | 1 | 2 | 3 | 4 | 5 | 6 |
|---|---|---|---|---|---|---|
| 1 | — | — | 55 | 52 | — | — |
| 2 | — | 46 | 50 | 42 | 41 | — |
| 3 | 56 | 52 | 32 | 22 | 33 | 43 |
| 4 | 52 | 46 | 28 | 18 | 28 | 41 |
| 5 | — | 41 | 35 | 31 | 39 | — |
| 6 | — | — | 44 | 43 | — | — |

TABLE 2 The power (mW) input to the various heaters. A controller with a gain of 32 mW K$^{-1}$ is active. The horizontal location of the heaters is given in figure 2.

supplied to the various heaters. We suspect that this non-uniformity in power was caused by imperfections in the experimental apparatus, the actuators' attempt to combat these imperfections, and the relatively crude control of the heater power.

In order to verify that the convection suppression was, indeed, caused by the dynamic action of the controller and not by the redistribution of the heating rate along the bottom plate, we froze each heater's power at its time-averaged value. In other words, during the controlled experiments, we measured the time-averaged power to each heater, and then we turned the controller off and assigned to each heater the same average value as measured when the controller was active. In figures 7 and 8, the resulting $\Delta T^m_{max}$ values are denoted, respectively, as a star (*) and a hollow circle for the frozen power distributions at ($\bar{p} = 37$ mW/heater, $k_p = 70$ mW K$^{-1}$) and ($\bar{p} = 40$ mW/heater, $k_p = 32$ mW K$^{-1}$). Note that when the controller was off and the power distribution was 'frozen', almost the same values of $\Delta T^m_{max}$ were measured as when the bottom plate was uniformly heated (without control). The corresponding flow pattern was also similar to the one when the bottom flux was uniform – a single cell structure with the flow ascending in one half of the cylinder and descending in the other. This

suggests that the dynamic action of the controller rather than the redistribution of the heating rate was responsible for the suppression of convection.

Figure 9 depicts the time-averaged average bottom–top temperature difference, $\Delta\bar{T}_{BT}$, as a function of the time-averaged average power input to the heaters, $\bar{p}$, and various control gains, $k_p = 0$ (no control), 70, and 100 mW K$^{-1}$. Note that when the controller was active, $\Delta\bar{T}_{BT}$ (solid line in figure 9) is nearly a linear function of $\bar{p}$ consistent with predominantly conductive heat transfer. In the uncontrolled case, as convection gained importance, there was a clear change of slope. In the controlled case, there is no such change of slope. Also note that when $\bar{p} > 32$ mW/heater, $\Delta\bar{T}_{BT}$ is larger in the controlled case than in the uncontrolled case. This is again consistent with the controller maintaining a mostly conductive state which offers a higher thermal resistance than the convective state present in the uncontrolled case.

Figure 10 depicts the maximum time-averaged bottom temperature difference, $\Delta T_B$, as a function of the time-averaged average power input to the heaters, $\bar{p}$, and various control gains, $k_p = 0$, (no control), 70, and 100 mW K$^{-1}$. In the uncontrolled case (solid circles), $\Delta T_B$ increases nearly linearly as a function of $\bar{p}$. In the presence of the controller and for the same average power, the controller maintains smaller values of $\Delta T_B$ (dashed line) than in the uncontrolled case. Again, this is consistent with the controller's effort to maintain a predominantly conductive state.

Thus far, we have described the controller's action when the power was gradually increased with the controller being active. In figure 11, we examine the controller's ability to suppress established convection. Figure 11 depicts the minimum and maximum midheight temperatures measured by the diodes 7 (light line) and 16 (heavy line) as functions of time. The nominal power is 40 mW/heater. Initially, as the power increased, the controller was not active and time-independent convection began in the cylinder. At time $t = 9.54$ h, a controller with gain 100 mW K$^{-1}$ was activated. Witness the significant reduction in the temperature difference. In the absence and the presence of the controller, $\Delta T^m_{max} = 6.4$ °C and 0.8 °C, respectively. Figure 11 illustrates that the controller can suppress established convection.

When the controller was active, both the temperatures and the heater powers oscillated as functions of time. For low controller gains, these oscillations were of relatively small amplitude and were the result of the controller's reaction to naturally occurring temperature fluctuations. For example, a sample of the fluctuations experienced by two diode–actuator pairs in the time interval $13\text{ h} < t < 16\text{ h}$ are depicted in the inserts in figure 11. In order to make the temperature fluctuations visible, it was necessary to significantly magnify the scale of the figure. In the absence of the controller ($t < 9.54$ h), there were no power oscillations and the diode temperature oscillations were much smaller than in the controller's presence.

When the controller gain was increased above 100 mW K$^{-1}$, the controller itself introduced oscillatory behaviour and the amplitude of the oscillations increased. Figure 12 shows the chain of events as the heaters' nominal power was decreased from 50 mW/heater to 40 mW/heater in the presence of a controller with a proportional gain $k_p = 200$ mW/C. Figure 12(*a*) depicts as functions of time, the temperature measured by diode 2 and the power to heater 2 and figure 12(*b*) depicts the temperature measured by thermocouple (A) installed on the heated surface. At a nominal power of 50 mW/heater, the oscillations had a relatively low amplitude. As the power was reduced to 40 mW/heater, the amplitude of the oscillations had considerably increased. Nevertheless, in the oscillatory regime, the time-averaged maximum difference of 0.8 K in midheight temperatures was significantly smaller than the temperature difference of 6.4 K in the controller's absence.

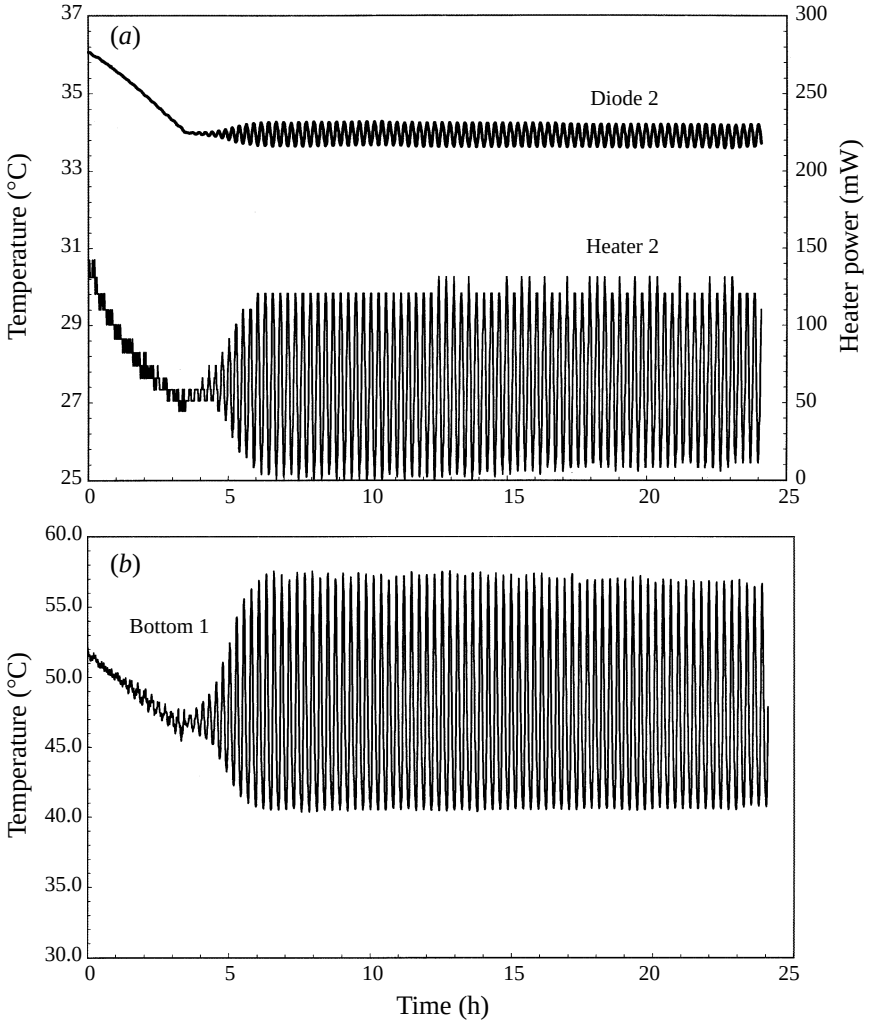


FIGURE 12. The nominal power is decreased from 50 mW/heater to 40 mW/heater and remained at 40 mW/heater. The controller gain is 0.2 W $K^{-1}$. (*a*) The temperature recorded by diode 2, the power supplied to heater 2, and (*b*) the bottom temperature recorded by thermocouple 1 are depicted as functions of time.

Both the temperatures and power oscillated at a frequency of about $1.04 \times 10^{-3}$ Hz. The frequency of the oscillations was insensitive to the nominal power, and similar frequencies were observed at different powers. The oscillation amplitude varied strongly with the nominal power setting. Figure 13 depicts to r.m.s. of the temperature oscillations (diode 2) as a function of the power input when $k_p = 200$ mW $K^{-1}$. Note that as the power increased, the amplitude of the oscillations initially increased, reached a maximum, and then decreased. We suspect that the oscillatory behaviour at high controller gains was caused by the controller over-reacting to the disturbance. Similar oscillatory behaviour for high controller gains and high-Prandtl-number fluids was predicted by Tang & Bau (1994) for controlled convection in an infinite fluid layer. The reduction in the r.m.s. of the oscillations at high powers (figure 13) may have been caused by the saturation of the actuators.

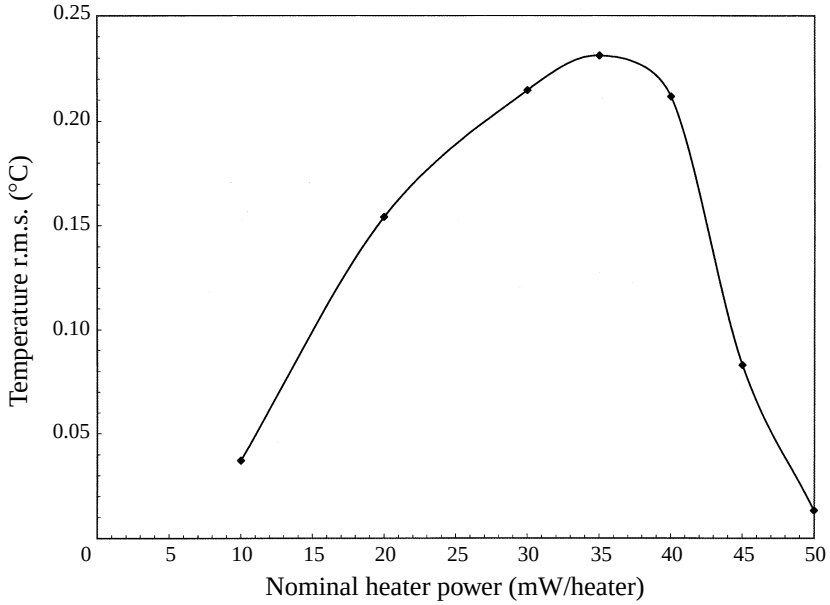


FIGURE 13. The amplitude of the temperature oscillations recorded by diode 2 as a function of the nominal power input. $k_p = 0.2$ W K$^{-1}$.

## 5. Conclusions

The significance of this study is that it provides an experimental demonstration that through the use of sensors and actuators, one can control three-dimensional Rayleigh–Bénard convection. Unfortunately, the degree of stabilization obtained in the experiments falls far short of Tang & Bau's (1994) theoretical prediction that the critical Rayleigh number for the onset of convection in an infinite fluid layer can be postponed by as much as an order of magnitude. The inability of the controller to achieve as good a performance as predicted may have been caused by imperfections in the experimental apparatus, errors in predicting the correct set temperature, poor resolution of the power control, saturation of the actuators, conduction through the sidewall, or an insufficient number of sensors and actuators. For example, the theoretical work assumed that the actuators and sensors were continuously distributed in space while in the experiment it was necessary to use a finite number of sensors and actuators. However, the very fact that we were successful in affecting the flow patterns suggests that additional gains can be made by optimizing the control strategy and refining the experimental apparatus.

This work was supported, in part, by grant CTS-9632237 from the National Science Foundation.

## REFERENCES

DAVIS, S. H. 1976 The stability of time periodic flows. *Ann. Rev. Fluid Mech.* **8**, 57–74.

DONNELLY, R. J. 1990 Externally modulated hydrodynamic systems. In *Nonlinear Evolution of Spatio-Temporal Structures in Dissipative Continuous Systems* (ed. F. H. Busse & L. Kramer), pp. 31–43. Plenum.

HOWLE, L. E. 1997 Control of Rayleigh–Bénard convection in a small aspect ratio container. *Intl J. Heat Mass Transfer* **40**, 817–822.

KELLY, R. E. 1992 Stabilization of Rayleigh–Bénard convection by means of a slow nonplanar oscillatory flow. *Phys. Fluids* A, **4**, 647–648.

KELLY, R. E. & HU, H. C. 1993 The onset of Rayleigh–Bénard convection in a nonplanar oscillatory flow. *J. Fluid Mech.* **249**, 373–390.

MÜLLER, G., NEUMANN, G. & WEBBER, W. 1984 Natural convection in vertical Bridgman configurations. *J. Cryst. Growth* **70**, 78–93.

NEUMANN, G. 1990 Three-dimensional numerical simulation of buoyancy-driven convection in vertical cylinders heated from below. *J. Fluid Mech.* **214**, 559–578.

ROPPO, M. N., DAVIS, S. H. & ROSENBLAT, S. 1984 Bénard convection with time-periodic heating. *Phys. Fluids* **27**, 796–803.

SINGER, J. & BAU, H. H. 1991 Active control of convection. *Phys. Fluids* A **3**, 2859–2865.

SINGER, J., WANG, Y.-Z. & BAU, H. H. 1991 Controlling a chaotic system. *Phys. Rev. Lett.* **66**, 1123–1125.

TANG, J. 1996 Active control of Rayleigh–Bénard convection. PhD thesis, University of Pennsylvania.

TANG, J. & BAU, H. H. 1993*a* Stabilization of the no-motion state in Rayleigh–Bénard convection through the use of feedback control. *Phys. Rev. Lett.* **70**, 1795–1798.

TANG, J. & BAU, H. H. 1993*b* Feedback control stabilization of the no-motion state of a fluid confined in a horizontal, porous layer heated from below. *J. Fluid Mech.* **257**, 485–505.

TANG, J. & BAU, H. H. 1994 Stabilization of the no-motion state in the Rayleigh–Bénard problem. *Proc. R. Soc. Lond.* A **447**, 587–607.

TANG, J. & BAU, H. H. 1995 Stabilization of the no-motion state of a horizontal fluid layer heated from below with Joule heating. *Trans. ASME: J. Heat Transfer* **117**, 329–333.

WANG, Y.-Z., SINGER, J. & BAU, H. H. 1992 Controlling chaos in thermal convection loop. *J. Fluid Mech.* **237**, 479–498.

YUEN, P. 1997 Dynamics and control of flow in a thermal convection loop. PhD thesis, University of Pennsylvania.

YUEN, P. & BAU, H. H. 1996 Rendering a subcritical bifurcation supercritical. *J. Fluid Mech.* **317**, 91–109.